

# General Self-Prediction Enhancement for Spiking Neurons

Zihan Huang<sup>1</sup> Zijie Xu<sup>1</sup> Yifan Huang<sup>1</sup> Shanshan Jia<sup>1</sup> Tong Bu<sup>1</sup> Yiting Dong<sup>1</sup> Wenxuan Liu<sup>1</sup>  
 Jianhao Ding<sup>1</sup> Zhaofei Yu<sup>1</sup> Tiejun Huang<sup>1</sup>

## Abstract

Spiking Neural Networks (SNNs) are highly energy-efficient due to event-driven, sparse computation, but their training is challenged by spike non-differentiability and trade-offs among performance, efficiency, and biological plausibility. Crucially, mainstream SNNs ignore predictive coding, a core cortical mechanism where the brain predicts inputs and encodes errors for efficient perception. Inspired by this, we propose a self-prediction enhanced spiking neuron method that generates an internal prediction current from its input–output history to modulate membrane potential. This design offers dual advantages, it creates a continuous gradient path that alleviates vanishing gradients and boosts training stability and accuracy, while also aligning with biological principles, which resembles distal dendritic modulation and error-driven synaptic plasticity. Experiments show consistent performance gains across diverse architectures, neuron types, time steps, and tasks demonstrating broad applicability for enhancing SNNs.

## 1. Introduction

Spiking Neural Networks (SNNs) constitute a biologically plausible class of neural network models that communicate through discrete, time-encoded spikes (Maass, 1997). Unlike conventional Artificial Neural Networks (ANNs), which rely on continuous activation values, SNNs activate only when a neuron’s membrane potential crosses a firing threshold (Gerstner et al., 2014). This event-driven mechanism leads to highly sparse computation, making SNNs exceptionally energy-efficient for deploying intelligent systems on resource-constrained edge hardware (Li et al., 2024). Recent neuromorphic platforms such as Loihi (Davies et al., 2018), TrueNorth (DeBole et al., 2019), Darwin (Ma et al., 2017) and Tianjic (Pei et al., 2019) have demonstrated the

potential of SNNs to enable low-power, real-time inference. Despite these benefits, training high performance SNNs remains a big challenge. The core issue stems from the binary, non-differentiable nature of spike events, which is not suitable for standard backpropagation. Moreover, simulating temporal dynamics during training often demands substantial memory and computational overhead.

To circumvent these limitations, researchers have developed two main paradigms for building high-performance SNNs: direct training and ANN-to-SNN conversion. Direct training approaches attempt to learn SNN weights end-to-end by approximating gradients through surrogate gradient functions (Neftci et al., 2019; Duan et al., 2022), or by leveraging biologically motivated rules like spike-timing-dependent plasticity (STDP) (Masquelier & Thorpe, 2007; Masquelier et al., 2008; 2009). While these methods aim to fully exploit the temporal information of spiking dynamics, they often suffer from long convergence times, and accuracy gaps on benchmark datasets (Gygax & Zenke, 2024). In contrast, ANN-to-SNN conversion first trains a high-accuracy ANN using standard deep learning methods and then converting it into an SNN that approximates its input–output behavior through rate-based or temporal coding schemes (Cao et al., 2015; Rueckauer et al., 2017; Han et al., 2020; Li et al., 2021; Bu et al., 2022; Huang et al., 2024b). Although the converted SNN is still more energy-efficient than the original ANN, it usually incurs a non-negligible accuracy drop especially under tight latency. Meanwhile, the resulting SNN merely replicates ANN functionality without leveraging temporal spiking dynamics, and thus lacks biological interpretability.

Despite those advances in SNNs, they largely ignore a core principle of cortical computation: the brain predicts sensory inputs and computes deviations from prediction errors. Evidence shows that individual auditory neurons fire selectively to omitted expected sounds, directly signaling prediction errors at the single-neuron level (Lao-Rodríguez et al., 2023; 2025). Pre-activated neural templates resembling actual stimulus responses further support this predictive coding framework (SanMiguel et al., 2013), with recent work identifying neurons specifically tuned to negative prediction errors (Yaron et al., 2025). Beyond population-level mechanisms, prediction may also occur within single neurons.

<sup>1</sup>Peking University, Beijing, China. Correspondence to: Zhaofei Yu <xxxx>.

(Hawkins & Ahmad, 2016) proposed that dendritic branches act as independent pattern detectors, enabling internal predictions. This aligns with models where dendrites predict somatic activity, and local prediction errors drive synaptic plasticity (Urbanczik & Senn, 2014; Brea et al., 2016; Sacramento et al., 2018). Yet such biologically grounded, neuron-intrinsic predictive mechanisms are missing from most SNNs.

Inspired by these, we propose a self-prediction enhanced spiking neuron method that is compatible with most spiking neuron model within arbitrary spiking neural networks. The core idea is to enable each neuron to leverage its own historical inputs and outputs to internally generate a self-prediction error to further generate prediction current, which dynamically modulates its membrane potential as an auxiliary input current. This prediction current can pre-activate expected spiking events and generate a prediction error signal when the actual output deviates from the prediction, thereby facilitating or suppressing subsequent spike emissions. Our main contributions are summarized as follows:

- We propose a prediction current based on self-prediction error and demonstrate how it enhances arbitrary spiking neurons.
- We provide a thorough analysis of the self-prediction enhanced neuron from the perspectives of dynamics, gradient propagation, and biological plausibility.
- We evaluate our method on image classification tasks across various network architectures, spiking neuron models, and datasets, demonstrating its effectiveness.
- We further validate our approach in sequential classification tasks and reinforcement learning tasks with multiple neuron types to verify its broad applicability and robustness.

## 2. Related Works

### 2.1. Direct Training of SNNs

Recent years have witnessed significant progress in directly training deep SNNs. Pioneering works such as STBP (Wu et al., 2018), SuperSpike (Zenke & Ganguli, 2018), and SLAYER (Shrestha & Orchard, 2018) introduced surrogate gradient methods to avoid the non-differentiability of spike emission, enabling end-to-end supervised learning. Subsequent efforts further enhanced SNN performance through more expressive neuron models such as learnable membrane time constants (Fang et al., 2021b), adaptive firing thresholds with moderate dropout (Wang et al., 2022), complementary LIF dynamics to mitigate temporal gradient vanishing (Huang et al., 2024a), and unified gated LIF frameworks that integrate diverse biological features (Yao

et al., 2022). Concurrently, architectural advances in residual architectures such as Spiking ResNet (Hu et al., 2021), SEW ResNet (Fang et al., 2021a), and MS-ResNet (Hu et al., 2024) have mitigated degradation and enabled stable training of deep networks; Meanwhile, attention-based models including Spikformer (Zhou et al., 2022), Spike-driven Transformer (Yao et al., 2023), and QKFormer (Zhou et al., 2024), have successfully integrated self-attention mechanisms into the spiking paradigm.

Despite these advances, most approaches prioritize engineering performance over biological interpretability. To bridge this gap, researchers have incorporated recurrent or feedback connections to emulate the brain’s intrinsic recurrent processing (Liang & Hu, 2015; Liang et al., 2015; Yin et al., 2020; Liao & Poggio, 2016). While biologically inspired, such recurrent SNNs often suffer from high computational costs, slow convergence, and difficulty in scaling to large architectures, limiting their practical utility. This trade between efficiency and plausibility calls for a new neuron-level mechanism that intrinsically integrates predictive feedback dynamics without relying on costly global recurrence.

### 2.2. Predictive Coding Theory

Predictive coding (PC) aims to minimizes redundancy by propagating prediction errors rather than raw sensory signals (Elias, 2003). In neuroscience, PC has been formalized as a hierarchical inference framework where higher areas generate predictions and lower areas compute local mismatches (Huang & Rao, 2011; Spratling, 2017). A growing body of work indicate that prediction operates not only at the network level but within individual neurons (Hawkins & Ahmad, 2016). Consistent with this view, several computational models formalize dendritic processing as a form of predictive coding, where basal or apical dendrites learn to predict somatic activity, and synaptic plasticity is driven by local prediction errors (Urbanczik & Senn, 2014; Brea et al., 2016; Sacramento et al., 2018).

Predictive coding has also inspired several SNN models, such as PC-SNN (Lan et al., 2022), which uses firing time prediction errors for supervised learning, and SNN-PC (Lee et al., 2024), which employs dedicated positive and negative error neurons for unsupervised reconstruction. (Yin et al., 2018) point out that autapses connections formed by pyramidal cells, where the axon synapses onto the neuron’s own dendrites or soma, are a key component of neural circuitry. However, none of them embed the prediction process within the SNN neuron itself by leveraging its own past inputs and outputs for self-prediction, which can effectively improve efficiency compared to layer-level recurrence prediction error computation.

To address these gaps, we propose a self-prediction paradigm applicable to diverse spiking neuron models,

wherein each neuron uses its past inputs and outputs to compute an online local prediction error signal.

### 3. Preliminaries

#### 3.1. Neurons in SNNs

In SNNs, neuron models serve as the fundamental computational units responsible for encoding, transmitting, and processing temporal information through discrete spikes. Among various models, the Leaky Integrate-and-Fire (LIF) neuron is the most widely adopted due to its balance between biological plausibility and computational efficiency.

The dynamics of a LIF neuron layer  $l$  at time-step  $t$  can be formulated as follows:

$$\mathbf{I}^l[t] = \mathbf{x}^{l-1}[t] = \mathbf{W}^l[t] \mathbf{s}^{l-1}[t], \quad (1)$$

$$\mathbf{m}^l[t] = (1 - \frac{1}{\tau^l}) \mathbf{v}^l[t-1] + \frac{1}{\tau^l} \mathbf{I}^l[t], \quad (2)$$

$$\mathbf{s}^l[t] = \text{H}(\mathbf{m}^l[t] - \theta^l), \quad (3)$$

where  $\mathbf{I}^l[t]$  denotes the synaptic input current, which equal to the weighted output  $\mathbf{x}^{l-1}[t]$  of last layer,  $\mathbf{W}^l$  is the weight matrix,  $\mathbf{s}^{l-1}[t]$  is the spike vector from the previous layer,  $\mathbf{m}^l[t]$  is the membrane potential before reset,  $\tau^l$  is the membrane time constant,  $\theta^l$  is the firing threshold, and  $\text{H}(\cdot)$  is the Heaviside step function. After spiking, the membrane potential  $\mathbf{v}^l[t]$  is reset. Two common reset strategies are hard reset and soft reset as in Eq. (4) and (5).

$$\mathbf{v}^l[t] = \mathbf{m}^l[t] - \mathbf{s}^l[t](\mathbf{m}^l[t] - v_{\text{reset}}), \quad (4)$$

$$\mathbf{v}^l[t] = \mathbf{m}^l[t] - \theta^l \mathbf{s}^l[t], \quad (5)$$

where  $v_{\text{reset}}$  is a fixed reset potential often set to 0.

The Integrate-and-Fire (IF) neuron is a simplified variant of the LIF model that omits membrane potential leakage. Its update rule replaces Eq. (2) with:

$$\mathbf{m}^l[t] = \mathbf{v}^{l-1}[t] + \mathbf{I}^l[t]. \quad (6)$$

This model assumes perfect integration of inputs until a spike is emitted, making it computationally efficient but less biologically realistic.

The Parametric Leaky Integrate-and-Fire (PLIF) neuron extends the LIF model by treating the membrane time constant  $\tau^l$  as a learnable parameter rather than a fixed hyperparameter. This allows the network to adapt the temporal dynamics of each neuron during training, enhancing its capacity to capture diverse temporal patterns and improving overall learning performance.

The Complementary Leaky Integrate-and-Fire (CLIF) neuron introduces an auxiliary complementary membrane potential to enrich neuronal dynamics. Specifically, CLIF

employs soft reset and removes input decay. Its dynamics are defined as:

$$\mathbf{m}^l[t] = (1 - \frac{1}{\tau^l}) \mathbf{v}^l[t-1] + \mathbf{I}^l[t], \quad (7)$$

$$\mathbf{s}^l[t] = \text{H}(\mathbf{m}^l[t] - \theta^l), \quad (8)$$

$$\mathbf{m}_c^l[t] = \mathbf{m}_c^l[t-1] \cdot \sigma(\frac{1}{\tau^l} \mathbf{m}^{l-1}[t]) + \mathbf{s}^l[t], \quad (9)$$

$$\mathbf{v}^l[t] = \mathbf{m}^l[t] - \mathbf{s}^l[t](\theta^l + \sigma(\mathbf{m}_c^l[t])), \quad (10)$$

where  $\mathbf{m}_c^l[t]$  is a complementary membrane state that accumulates spike history modulated by a sigmoid gate  $\sigma(\cdot)$ , and the reset magnitude is dynamically adjusted based on both the threshold and this complementary state.

Together, various neuron models represent a spectrum of design choices in SNNs, ranging from simplicity and efficiency to enhanced temporal expressivity and adaptive dynamics.

#### 3.2. SNN Training with Surrogate Gradient

In SNNs employing common neuron models such as IF, LIF, and PLIF, backpropagation through time follows the chain rule. As suggested by (Neftci et al., 2019), removing the gradient path through the reset terms in Eqs. (4) and (5) improves training stability and overall network performance. The resulting gradient computations are as follows:

$$\frac{\partial L}{\partial \mathbf{I}^l[t]} = \frac{\partial L}{\partial \mathbf{m}^l[t]} \frac{\partial \mathbf{m}^l[t]}{\partial \mathbf{I}^l[t]}, \quad (11)$$

$$\frac{\partial L}{\partial \mathbf{m}^l[t]} = \frac{\partial L}{\partial \mathbf{s}^l[t]} \frac{\partial \mathbf{s}^l[t]}{\partial \mathbf{m}^l[t]} + \frac{\partial L}{\partial \mathbf{m}^l[t+1]} \frac{\partial \mathbf{m}^l[t+1]}{\partial \mathbf{m}^l[t]}. \quad (12)$$

The term  $\frac{\partial \mathbf{s}^l[t]}{\partial \mathbf{m}^l[t]}$  is non-differentiable because  $\mathbf{s}^l[t] = \text{H}(\mathbf{m}^l[t] - \theta^l)$  involves the Heaviside step function. To enable gradient-based optimization, surrogate gradient methods replace this derivative with a smooth, differentiable approximation. A common choice is the sigmoid function:

$$\frac{\partial \mathbf{s}^l[t]}{\partial \mathbf{m}^l[t]} \approx \sigma'(\mathbf{m}^l[t] - \theta^l), \quad (13)$$

where  $\sigma(x) = \frac{1}{1+e^{-kx}}$ ,  $k > 0$ .  $k$  controls the steepness of the surrogate, larger  $k$  yields a closer approximation to the true Heaviside function. With this substitution, gradients can be propagated through spiking layers, enabling end-to-end training of SNNs while preserving their discrete, event-driven nature in the forward pass.

### 4. Method

In this section, we first introduce our self-prediction enhanced neuron method from the perspective of predictive coding and provide a detailed analysis of its dynamics. We

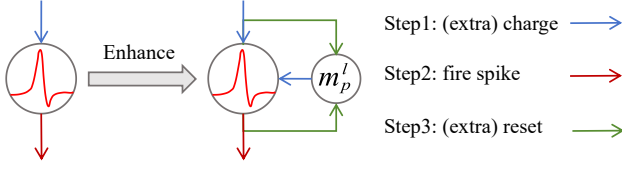


Figure 1. Left: original neuron, Right: our proposed self-prediction enhanced neuron. Neurons operate in the sequence of charging, firing, and resetting at each time-step.

then explain why self-prediction enhances neuronal efficacy based on gradient analysis, and finally offer a biologically plausible interpretation of the proposed mechanism.

#### 4.1. Self-prediction Enhanced Spiking Neurons

Predictive coding theory posits that the brain continuously generates internal predictions about sensory inputs and updates its internal model using the prediction error, which is the discrepancy between actual observations and predictions. At the neuronal level, many neurons exhibit pre-activate activity prior to an expected event, which can be interpreted as a prediction about whether a spike should occur at the current time-step.

Inspired by this principle, we propose that if a spiking neuron can locally predict its next state based on its own history of inputs and outputs, and inject this prediction into its dynamics as an auxiliary current, it can simultaneously enhance both biological plausibility and computational performance. A schematic illustration of the self-prediction enhanced neuron is shown in Figure 1. Specifically, we introduce a weak prediction current  $m_p^l[t]$ , which is added to the original input current to dynamically modulate the membrane potential. The design objectives of this current are as follows:

- (1) When a spike is predicted, the membrane potential is slightly elevated to bring it close to but still below the firing threshold, thereby pre-activating the neuron in anticipation of the expected event;
- (2) When no spike is predicted, moderately lower the membrane potential to suppress noise-induced unexpected spikes;
- (3) When a spike is predicted but not emitted, generate a positive prediction error to increase sensitivity to similar future inputs;
- (4) When no spike is predicted but one is emitted, generate a negative prediction error to suppress over-responsive behavior in the future.

Begin by regarding prediction error term as:

$$\mathbf{x}^{l-1}[t] - \mathbf{s}^l[t]/\tau^l, \quad (14)$$

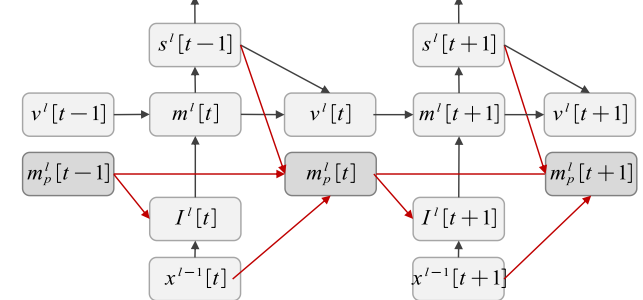


Figure 2. Forward propagation pathway of the self-prediction enhanced LIF neuron. The red lines indicate the additional forward path associated with self-prediction.

where,  $\tau^l$  is the neuronal membrane time constant. The division by  $\tau^l$  compensates for the exponential decay of input currents, rendering  $\mathbf{s}^l[t]/\tau^l$  a reasonable estimate of the effective contribution of the current spike to the membrane potential.

Consider a standard spiking neuron in layer  $l$ , with raw input  $\mathbf{x}^{l-1}[t]$  and binary output  $\mathbf{s}^l[t] \in \{0, 1\}$ . We enhance the input by introducing the prediction current  $\mathbf{m}_p^l[t]$ :

$$\mathbf{I}^l[t] = \mathbf{x}^{l-1}[t] + \mathbf{m}_p^l[t-1]. \quad (15)$$

The prediction current is updated dynamically via a low-pass filter that computes a moving average of the prediction error:

$$\mathbf{m}_p^l[t] = (1 - \tau_p^l)\mathbf{m}_p^l[t-1] + \tau_p^l(\mathbf{x}^{l-1}[t] - \frac{\mathbf{s}^l[t]}{\tau^l}), \quad (16)$$

where  $\tau_p^l \in (0, 1)$  controls the update rate of the prediction current.

Specifically, taking a hard-reset LIF neuron as an example, the full dynamics of the enhanced neuron can be written as:

$$\mathbf{I}^l[t] = \mathbf{x}^{l-1}[t] + \mathbf{m}_p^l[t-1], \quad (17)$$

$$\mathbf{m}^l[t] = (1 - \frac{1}{\tau^l})\mathbf{v}^{l-1}[t] + \frac{1}{\tau^l}\mathbf{I}^l[t], \quad (18)$$

$$\mathbf{s}^l[t] = \mathbf{H}(\mathbf{m}^l[t] - \theta^l), \quad (19)$$

$$\mathbf{v}^l[t] = \mathbf{m}^l[t] - \mathbf{s}^l[t](\mathbf{m}^l[t] - v_{reset}), \quad (20)$$

$$\mathbf{m}_p^l[t] = (1 - \tau_p^l)\mathbf{m}_p^l[t-1] + \tau_p^l(\mathbf{x}^{l-1}[t] - \frac{\mathbf{s}^l[t]}{\tau^l}). \quad (21)$$

The forward propagation pathway is shown in Figure 2.

Now analyzing the prediction error term  $\mathbf{x}^{l-1}[t] - \mathbf{s}^l[t]/\tau^l$  in Eq.(21) from a dynamical perspective:

- (1) **If the current input is high and a spike is emitted,** i.e.,  $\mathbf{x}^{l-1}[t]$  is large and  $\mathbf{s}^l[t] = 1$ . This implicitly indicates that the prediction at the current time-step is correct and

that the neuron tends to predict a spike at the next time-step. Typically,  $(x^{l-1}[t] - s^l[t]/\tau^l)$  should be close to zero but slightly positive. This is because, in previous time-steps,  $x^{l-1}[t]$  must have exceeded  $s^l[t]/\tau^l$  to trigger the spike. The predictive current raise the membrane potential, thereby moderately increasing the likelihood of the expected spike and promoting its stable generation.

(2) **If the current input is low and no spike is emitted**, i.e.,  $x^{l-1}[t]$  is small and  $s^l[t] = 0$ . This implicitly indicates that the prediction at the current time-step is correct and that the neuron tends to predict no spike at the next time-step. The error term should be close to zero or negative, and the predictive current tends toward zero or becomes slightly negative, keeping the membrane potential at a low level and effectively suppressing noise-induced spurious spikes. If the error term is slightly greater than zero and the input remains low in subsequent time-steps, no spike will be emitted. Due to the decay mechanism, both the membrane potential  $v^l[t]$  and the predictive current  $m_p^l[t]$  remain at low levels.

(3) **If the current input is high but no spike is emitted**, i.e.,  $x^{l-1}[t]$  is large yet  $s^l[t] = 0$ . This indicates a prediction error that a spike was expected but did not occur. In this case,  $m_p^l[t]$  increases in the positive direction, amplifying the missed signal in subsequent time-steps and driving the network to enhance its sensitivity to inputs.

(4) **If the current input is low yet an unexpected spike occurs**, i.e.,  $x^{l-1}[t]$  is small but  $s^l[t] = 1$ . This also reflects a prediction error that a spike occurred when none was expected. Consequently,  $m_p^l[t]$  is updated in the negative direction, encouraging the network to learn to suppress such error responses in the subsequent time-step.

Moreover, the moving average form in Eq. (21) offers two key advantages. One is that it establishes a learnable temporal window that links past inputs to current outputs, enabling short-term prediction; and Another is the low-pass filtering property suppresses high-frequency noise, allowing the prediction current to robustly reflect genuine patterns.

## 4.2. Gradient Analysis

For a typical spiking neuron model, the gradient with respect to the membrane potential  $m^l[t]$  as in Eqs. (11) and (12) can be expanded over time as follows:

$$\frac{\partial L}{\partial m^l[t]} = \sum_{i=t}^T \frac{\partial L}{\partial s^l[i]} \frac{\partial s^l[i]}{\partial m^l[i]} \prod_{j=t}^{i-1} \frac{\partial m^l[j+1]}{\partial m^l[j]}. \quad (22)$$

However, if few spike occurs at time-step  $t$ ,  $\frac{\partial s^l[i]}{\partial m^l[i]}$  becomes very sparse, leading to minimal gradients flowing back to  $m^l[t]$ . This results in limited information being propagated back to  $x^{l-1}[t]$ .

To address this issue, our proposed self-prediction enhanced

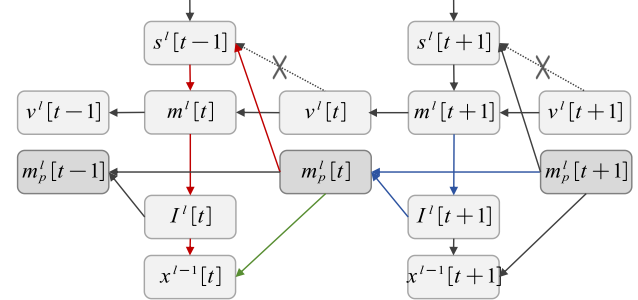


Figure 3. Backward propagation pathway of the self-prediction enhanced LIF neuron. The blue and green lines form the first additional gradient path, and the blue and red lines form the second additional gradient path. The dashed lines indicate paths that are detached from the computational graph.

neuron model introducing a predictive auxiliary state  $m_p^l[t]$ . The gradients for this enhanced model are given by:

$$\frac{\partial L}{\partial x^{l-1}[t]} = \frac{\partial L}{\partial m^l[t]} \frac{\partial m^l[t]}{\partial x^{l-1}[t]} + \frac{\partial L}{\partial m_p^l[t]} \frac{\partial m_p^l[t]}{\partial x^{l-1}[t]}, \quad (23)$$

$$\begin{aligned} \frac{\partial L}{\partial m^l[t]} = & \frac{\partial L}{\partial s^l[t]} \frac{\partial s^l[t]}{\partial m^l[t]} + \frac{\partial L}{\partial m^l[t+1]} \frac{\partial m^l[t+1]}{\partial m^l[t]} \\ & + \frac{\partial L}{\partial m_p^l[t]} \frac{\partial m_p^l[t]}{\partial s^l[t]} \frac{\partial s^l[t]}{\partial m^l[t]}, \end{aligned} \quad (24)$$

$$\begin{aligned} \frac{\partial L}{\partial m_p^l[t]} = & \frac{\partial L}{\partial m^l[t+1]} \frac{\partial m^l[t+1]}{\partial m_p^l[t]} \\ & + \frac{\partial L}{\partial m_p^l[t+1]} \frac{\partial m_p^l[t+1]}{\partial m_p^l[t]}. \end{aligned} \quad (25)$$

Following (Neftci et al., 2019), we remove the gradient path through the reset terms, but we keep the gradient path from  $m_p^l[t]$  to  $s^l[t]$ . Compared to the original gradient,  $\frac{\partial L}{\partial x^{l-1}[t]}$  now includes two additional pathways, as shown in Figure 3:

**1. Direct pathway: via  $m_p^l[t] \rightarrow x^{l-1}[t]$ .** This direct path bypasses the current-time spike  $s^l[t]$  and membrane potential  $m^l[t]$ , thereby avoiding gradient fragmentation caused by the sparsity of spiking activity. At each time-step,  $m_p^l[t]$  can directly inherit gradients from both  $m_p^l[t+1]$  and  $m^l[t+1]$ . Consequently, even if the neuron fires at time  $t+1$ , the gradient information is well preserved. By strengthening the influence of future-time gradients on the current time-step, this mechanism enhances the stability of prediction.

**2. Indirect pathway:  $m_p^l[t] \rightarrow s^l[t] \rightarrow m^l[t] \rightarrow x^{l-1}[t]$ .** This indirect path leverages the predictive nature of the model to enable more comprehensive gradient flow. Notably, we do not decouple the computational graph between  $m_p^l[t]$  and  $s^l[t]$ . Unlike the reset mechanism which discards historical information, we treat the auxiliary state  $m_p^l[t]$  as a continuous and smooth memory unit. As shown in Eq. (21),

although the update of  $m_p^l[t]$  involves the spike  $s^l[t]$ , the prediction error is jointly regulated by both input and output. Gradients through this pathway are smoothly propagated via surrogate gradients, enabling the network to adaptively correct prediction errors.

As analyzed in Section 4.1, the magnitude of  $m_p^l[t]$  remains small when there is no prediction error, but increases when a prediction error occurs. In such cases, the self-prediction-enhanced neuron actively learns from this error. By maintaining gradient pathways associated with  $m_p^l[t]$ , the model better captures temporal dependencies and achieves improved overall performance.

### 4.3. Biological Interpretability

Our proposed self-prediction enhanced spiking neuron is not only inspired by the computational principles of predictive coding but also grounded in biological observations of real neuronal mechanisms. In particular, the model closely resembles the modulatory role of distal dendrites in pyramidal neurons.

In biological neural systems, distal dendritic compartments receive top-down inputs that typically do not directly elicit somatic spikes. Instead, they modulate the neuron’s response to feedforward inputs, which effectively implementing a local predictive mechanism. The prediction current  $m_p^l[t]$  in our model serves as a functional analog of this biological mechanism. It does not directly participate in spike generation but acts as a learnable, subthreshold modulatory signal. Based on the joint statistics of past inputs  $x^{l-1}[t]$  and outputs  $s^l[t]$ , it continuously estimates the expected membrane change at the next time-step and accordingly fine-tunes the prediction current. Bring it closer to the threshold when a spike firing is predicted, and farther away when no spike is expected, thereby enabling local self-prediction.

Moreover, the error-driven update rule for  $m_p^l[t]$  aligns closely with synaptic plasticity. In biological synapses, prediction errors, such as strong feedforward input failing to stimulate an expected somatic spike or spontaneous spiking in the absence of supportive input, are thought to trigger calcium-dependent plasticity mechanisms in dendrites that adjust synaptic efficacy to minimize future prediction errors. In our model, the bottom-up drive is simplified to a local prediction error  $x^{l-1}[t] - s^l[t]/\tau^l$ , which error effectively reflects the prediction of the membrane potential changes. The total predictive drive  $m_p^l[t]$  is then updated slowly and adaptively with a time constant  $\tau_p^l$ , the dynamic process that closely mirrors the low-pass filtering properties exhibited by dendritic compartments. Thus, our model provides a functionally plausible and concise abstraction of how spiking neurons can leverage simplified dendritic compartmentalization and implicit local learning rules to implement predictive coding.

In summary, the proposed self-prediction enhanced neuron implements local predictive coding in SNNs through a concise mechanism that mimics dendritic modulation and error-driven plasticity.

## 5. Experimental Results

To validate the effectiveness of our proposed self-prediction enhanced spiking neuron method, we first conducted a series of ablation studies on the CIFAR-10 dataset. These experiments systematically evaluated performance under various neuron types, network architectures, and time-step configurations, thoroughly demonstrating the method’s generality and effectiveness. Subsequently, we evaluated our approach on larger-scale datasets ImageNet-100 and ImageNet-1K, further confirming its strong generalization capability in complex scenarios. Additionally, we applied our method to the sequential CIFAR-10 task, showcasing its enhanced temporal modeling capacity. Finally, we tested the method in reinforcement learning tasks, verifying its broad applicability and robustness across diverse task settings.

### 5.1. Ablation on Classification Tasks

We first validate the effectiveness of our proposed method on the CIFAR-10 dataset. The experiments employ five network architectures, including Spiking CIFAR10Net, SEW ResNet-18, SEW ResNet-34, Spiking ResNet-18, and Spiking ResNet-34; and four spiking neuron models, including IF, LIF, PLIF, and CLIF neuron as detail in Section 3.1, trained under time-steps  $T = 4$  and  $T = 8$ .

For the SEW ResNet and Spiking ResNet families which is originally designed for ImageNet, when adapting them to CIFAR-10, we modify the first convolutional layer parameters, changing kernel size, stride, and padding from 7, 2, 3 to 3, 1, 1, respectively, and replace the initial max pooling layer with an identity mapping. For the spiking CIFAR10Net, all Conv2d layers use a kernel size of 3, stride of 1, and padding of 1, with 256 output channels. Each Conv2d layer is followed by a batch normalization layer and a spiking neuron layer. The final feature map is passed through two fully connected layers for classification. Detailed architecture configuration is provided in the appendix.

Notably, we employ the learnable parameter  $\tau_p^l$  in Eq.(16) per layer. For instance, in ResNet-18, this introduces only 18 additional parameters, which is negligible compared to the total number of network parameters.

The overall ablation results are presented in Table 1. The results show that our self-prediction enhancement yields significant performance improvements with LIF, PLIF, and CLIF neurons, and also achieves gains in most configurations with IF neurons. For the few cases where performance slightly degrades, we attribute this to two main factors: first,

Table 1. Ablation Study on CIFAR10 Classification Tasks. S-neuron stands for self-prediction enhanced neuron. eg. S-IF is the self-prediction enhanced IF neuron.

Network	Neuron	T	Accuracy	Network	Neuron	T	Accuracy
Spiking CIFAR10Net	IF	4,8	94.33,94.21	Spiking CIFAR10Net	PLIF	4,8	93.85,94.05
Spiking CIFAR10Net	S-IF	4,8	94.24↓,94.84↑	Spiking CIFAR10Net	S-PLIF	4,8	94.39↑,94.85↑
Spiking CIFAR10Net	LIF	4,8	93.54,93.60	Spiking CIFAR10Net	CLIF	4,8	94.20,94.23
Spiking CIFAR10Net	S-LIF	4,8	93.84↑,94.85↑	Spiking CIFAR10Net	S-CLIF	4,8	94.70↑,94.38↑
SEW ResNet18	IF	4,8	94.53,94.50	SEW ResNet34	IF	4,8	95.49,95.58
SEW ResNet18	S-IF	4,8	94.20↓,94.78↑	SEW ResNet34	S-IF	4,8	95.59↑,95.73↑
SEW ResNet18	LIF	4,8	94.99,95.04	SEW ResNet34	LIF	4,8	95.42,94.54
SEW ResNet18	S-LIF	4,8	95.04↑,95.56↑	SEW ResNet34	S-LIF	4,8	95.86↑,96.16↑
SEW ResNet18	PLIF	4,8	95.21,95.04	SEW ResNet34	PLIF	4,8	95.57,93.49
SEW ResNet18	S-PLIF	4,8	95.25↑,95.73↑	SEW ResNet34	S-PLIF	4,8	95.87↑,96.33↑
SEW ResNet18	CLIF	4,8	94.92,95.31	SEW ResNet34	CLIF	4,8	95.54,94.87
SEW ResNet18	S-CLIF	4,8	95.42↑,95.26↓	SEW ResNet34	S-CLIF	4,8	96.11↑,95.99↑
Spiking ResNet18	IF	4,8	94.93,95.16	Spiking ResNet34	IF	4,8	94.89,94.96
Spiking ResNet18	S-IF	4,8	94.98↑,95.42↑	Spiking ResNet34	S-IF	4,8	94.67↓,94.96
Spiking ResNet18	LIF	4,8	93.43,94.21	Spiking ResNet34	LIF	4,8	91.45,87.71
Spiking ResNet18	S-LIF	4,8	95.05↑,95.41↑	Spiking ResNet34	S-LIF	4,8	92.43↑,93.82↑
Spiking ResNet18	PLIF	4,8	94.26,94.30	Spiking ResNet34	PLIF	4,8	93.16,88.93
Spiking ResNet18	S-PLIF	4,8	95.05↑,95.43↑	Spiking ResNet34	S-PLIF	4,8	93.48↑,92.76↑
Spiking ResNet18	CLIF	4,8	95.16,95.52	Spiking ResNet34	CLIF	4,8	94.58,94.57
Spiking ResNet18	S-CLIF	4,8	95.29↑,95.67↑	Spiking ResNet34	S-CLIF	4,8	95.04↑,94.60↑

Table 2. Ablation Study on ImageNet100 and ImageNet1k Classification Tasks.

Dataset	Network	Neuron	T	Accuracy
ImageNet100	SEW ResNet34	LIF	4	65.80
	SEW ResNet34	S-LIF	4	69.06↑
	SEW ResNet34	PLIF	4	68.30
	SEW ResNet34	S-PLIF	4	68.94↑
ImageNet1k	SEW ResNet18	PLIF	4	64.25
	SEW ResNet18	S-PLIF	4	64.45↑

the IF neuron lacks an input decay mechanism, with its time constant fixed at  $\tau = 1$ , making it difficult to effectively balance the presynaptic input  $\mathbf{x}^{l-1}[t]$  and the postsynaptic spike output  $\mathbf{s}^l[t]$  in the predict error term  $\mathbf{x}^{l-1}[t] - \mathbf{s}^l[t]/\tau$  of Equation (14); this insight also suggests a promising direction for future refinement. Second, the performance gain of our method becomes more consistent and stable as the number of simulation time steps increases.

Subsequently, comprehensive considering training cost, we evaluate our method on the larger-scale datasets ImageNet-100 with SEW ResNet34 model and ImageNet-1K with SEW ResNet18 model to further demonstrate its generalization capability in complex scenarios. The results are summarized in Table 2, it clearly shows that the self-prediction enhanced LIF and PLIF neurons consistently outperforms the original neuron across all settings.

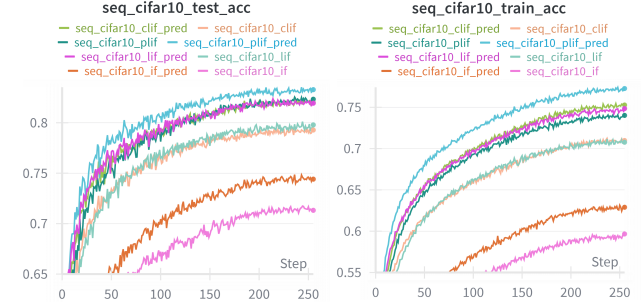


Figure 4. The training and testing accuracy curves of four spiking neuron models, IF, LIF, PLIF, and CLIF, along with their variants enhanced by self-prediction mechanisms.

## 5.2. Ablation on Sequence Classification Tasks

We believe our method is particularly effective for tasks involving long-term temporal dependencies. To verify this, we evaluate it on the Sequential CIFAR-10 task. In this setting, each time step feeds the network with one column of the input image, resulting in a total of  $T = 32$  time-steps that matches the image width. As shown in Figure 4, we train models using IF, LIF, PLIF, and CLIF neurons for 256 epochs and plot their training and test accuracy curves. Our self-prediction enhancement consistently yields noticeable improvements throughout the entire training process. Detailed best accuracy results are reported in Table 3.

Furthermore, we conduct an ablation study on detaching

Table 3. Ablation on Sequential CIFAR10 Classification Tasks.

Neuron/Acc.	base	self-pred(detach)	self-pred
IF	71.74	69.08 $\downarrow$	74.86 $\uparrow$
LIF	80.11	81.43 $\uparrow$	82.38 $\uparrow$
PLIF	82.54	83.03 $\uparrow$	83.52 $\uparrow$
CLIF	79.55	81.08 $\uparrow$	82.32 $\uparrow$

the gradient of the spike signal  $s^l[t]$  in the prediction error term  $\mathbf{x}^{l-1}[t] - s^l[t]/\tau$  when calculating  $\mathbf{m}_p^l[t]$ . The results show that preserving the full computational graph across  $\mathbf{m}_p^l[t]$  leads to better performance, which validates the rationale behind our gradient propagation design discussed in Section 4.2.

### 5.3. Ablation on Reinforcement Learning Tasks

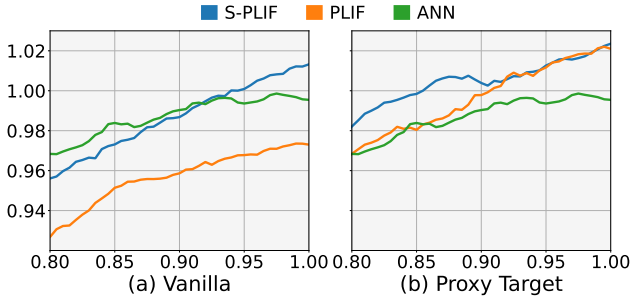


Figure 5. Normalized learning curves across all environments of the TD3 algorithm with different spiking neurons across all environments. The performance and training steps are normalized linearly based on ANN performance. Curves are uniformly smoothed for visual clarity.

Moreover, we conduct experiment on four changing reinforcement learning tasks from the MuJoCo (Todorov et al., 2012; Todorov, 2014) continuous control benchmarks including Ant-v4, HalfCheetah-v4, Hopper-v4, and Walker2d-v4. We combined PLIF and self-prediction enhanced PLIF(S-PLIF) neuron with the vanilla hybrid frameworks of the spiking actor networks (Tang et al., 2021), and the SOTA proxy target (PT) framework (Xu et al., 2025a). All experiments result are reimplemented results using the RL algorithm of Twin-delayed Deep Determination Policy Gradient (TD3) (Fujimoto et al., 2018) and we choose the hyperparameters as suggested in (Xu et al., 2025a).

Figure 5 shows the normalized learning curves across all 4 environments, and Table 4 reports the expected returns for each environment. We also report the average performance gain, defined as the average percentile improvement over ANNs, following the metric in Xu et al. (2025b). Our self-prediction enhancement consistently improves SNN performance in reinforcement learning (RL) tasks, even when integrated with state-of-the-art SNN-RL approaches such as proxy target frameworks. Notably, with this enhance-

Table 4. Max average returns over 5 random seeds with PLIF and S-PLIF spiking neurons, and the average performance gain against ANN baseline, where  $\pm$  denotes one standard deviation.

Environment	Frame	Neuron	Performance
Ant-v4	ANN	ReLU	4932 $\pm$ 1287
	Vanilla	PLIF	4912 $\pm$ 1009
	Vanilla	S-PLIF	4981 $\pm$ 607
	PT	PLIF	5259 $\pm$ 326
	PT	S-PLIF	5527 $\pm$ 151
	ANN	ReLU	10554 $\pm$ 561
HalfCheetah-v4	Vanilla	PLIF	9252 $\pm$ 520
	Vanilla	S-PLIF	9828 $\pm$ 594
	PT	PLIF	9219 $\pm$ 216
	PT	S-PLIF	9405 $\pm$ 597
	ANN	ReLU	3349 $\pm$ 151
	Vanilla	PLIF	3414 $\pm$ 122
Hopper-v4	Vanilla	S-PLIF	3462 $\pm$ 128
	PT	PLIF	3384 $\pm$ 100
	PT	S-PLIF	3380 $\pm$ 105
	ANN	ReLU	4050 $\pm$ 323
	Vanilla	PLIF	4003 $\pm$ 274
	Vanilla	S-PLIF	4271 $\pm$ 485
Walker2d-v4	PT	PLIF	4445 $\pm$ 217
	PT	S-PLIF	4497 $\pm$ 391
	ANN	ReLU	0.00%
	Vanilla	PLIF	-2.99%
	Vanilla	S-PLIF	0.74%
	PT	PLIF	1.20%
Overall	PT	S-PLIF	3.28%

ment, directly trained SNNs can achieve and sometimes even surpass ANN performances in RL tasks.

## 6. Conclusion

In this work, we proposed a self-prediction enhanced spiking neuron method, drawing inspiration from the brain’s predictive coding mechanisms. By enabling each neuron to generate an internal prediction current based on its own input-output history, our approach offers a simple yet effective way to modulate membrane potential dynamics. This design not only creates a continuous gradient path that mitigates vanishing gradients and significantly boosts training accuracy across diverse SNN architectures, neuron models, and tasks, but also aligns with biological principles of dendritic modulation and error-driven synaptic plasticity. Our comprehensive experiments on image classification, sequential classification, and reinforcement learning tasks consistently demonstrate the broad applicability and robustness of the proposed method, establishing it as a promising general enhancement for Spiking Neural Networks.

## Impact Statement

This paper presents work whose goal is to advance the field of Machine Learning. There are many potential societal consequences of our work, none which we feel must be specifically highlighted here.

## References

- Brea, J., Gaál, A. T., Urbanczik, R., and Senn, W. Prospective coding by spiking neurons. *PLoS computational biology*, 12(6):e1005003, 2016.
- Bu, T., Fang, W., Ding, J., Dai, P., Yu, Z., and Huang, T. Optimal ann-snn conversion for high-accuracy and ultra-low-latency spiking neural networks. In *International Conference on Learning Representations*, 2022.
- Cao, Y., Chen, Y., and Khosla, D. Spiking deep convolutional neural networks for energy-efficient object recognition. *International Journal of Computer Vision*, 113(1): 54–66, 2015.
- Davies, M., Srinivasa, N., Lin, T.-H., Chinya, G., Cao, Y., Choday, S. H., Dimou, G., Joshi, P., Imam, N., Jain, S., Liao, Y., Lin, C.-K., Lines, A., Liu, R., Mathaikutty, D., McCoy, S., Paul, A., Tse, J., Venkataraman, G., Weng, Y.-H., Wild, A., Yang, Y., and Wang, H. Loihi: a neuromorphic manycore processor with on-chip learning. *IEEE Micro*, 38(1):82–99, 2018. doi: 10.1109/MM.2018.112130359.
- DeBole, M. V., Taba, B., Amir, A., Akopyan, F., Andreopoulos, A., Risk, W. P., Kusnitz, J., Ortega Otero, C., Nayak, T. K., Appuswamy, R., Carlson, P. J., Cassidy, A. S., Datta, P., Esser, S. K., Garreau, G. J., Holland, K. L., Lekuch, S., Mastro, M., McKinstry, J., di Nolfo, C., Paulovicks, B., Sawada, J., Schleupen, K., Shaw, B. G., Klamo, J. L., Flickner, M. D., Arthur, J. V., and Modha, D. S. Truenorth: Accelerating from zero to 64 million neurons in 10 years. *Computer*, 52(5):20–29, 2019.
- Duan, C., Ding, J., Chen, S., Yu, Z., and Huang, T. Temporal effective batch normalization in spiking neural networks. In Koyejo, S., Mohamed, S., Agarwal, A., Belgrave, D., Cho, K., and Oh, A. (eds.), *Advances in Neural Information Processing Systems*, volume 35, pp. 34377–34390. Curran Associates, Inc., 2022.
- Elias, P. Predictive coding–i. *IRE transactions on information theory*, 1(1):16–24, 2003.
- Fang, W., Yu, Z., Chen, Y., Huang, T., Masquelier, T., and Tian, Y. Deep residual learning in spiking neural networks. *Advances in Neural Information Processing Systems*, 34:21056–21069, 2021a.
- Fang, W., Yu, Z., Chen, Y., Masquelier, T., Huang, T., and Tian, Y. Incorporating learnable membrane time constant to enhance learning of spiking neural networks. In *Proceedings of the IEEE/CVF international conference on computer vision*, pp. 2661–2671, 2021b.
- Fujimoto, S., Hoof, H., and Meger, D. Addressing function approximation error in actor-critic methods. In *International Conference on Machine Learning*, pp. 1587–1596. PMLR, 2018.
- Gerstner, W., Kistler, W. M., Naud, R., and Paninski, L. *Neuronal Dynamics: From Single Neurons to Networks and Models of Cognition*. Cambridge University Press, 2014.
- Gygax, J. and Zenke, F. Elucidating the theoretical underpinnings of surrogate gradient learning in spiking neural networks, 2024.
- Han, B., Srinivasan, G., and Roy, K. Rmp-snn: Residual membrane potential neuron for enabling deeper high-accuracy and low-latency spiking neural network. In *Proceedings of the IEEE/CVF Conference on Computer Vision and Pattern Recognition (CVPR)*, pp. 13558–13567, 2020.
- Hawkins, J. and Ahmad, S. Why neurons have thousands of synapses, a theory of sequence memory in neocortex. *Frontiers in neural circuits*, 10:23, 2016.
- Hu, Y., Tang, H., and Pan, G. Spiking deep residual networks. *IEEE Transactions on Neural Networks and Learning Systems*, 34(8):5200–5205, 2021.
- Hu, Y., Deng, L., Wu, Y., Yao, M., and Li, G. Advancing spiking neural networks toward deep residual learning. *IEEE transactions on neural networks and learning systems*, 36(2):2353–2367, 2024.
- Huang, Y. and Rao, R. P. Predictive coding. *Wiley Interdisciplinary Reviews: Cognitive Science*, 2(5):580–593, 2011.
- Huang, Y., Lin, X., Ren, H., Fu, H., Zhou, Y., Liu, Z., Pan, B., and Cheng, B. Clif: Complementary leaky integrate-and-fire neuron for spiking neural networks. *arXiv preprint arXiv:2402.04663*, 2024a.
- Huang, Z., Shi, X., Hao, Z., Bu, T., Ding, J., Yu, Z., and Huang, T. Towards high-performance spiking transformers from ann to snn conversion. In *Proceedings of the 32nd ACM international conference on multimedia*, pp. 10688–10697, 2024b.
- Lan, M., Xiong, X., Jiang, Z., and Lou, Y. Pc-snn: Supervised learning with local hebbian synaptic plasticity based on predictive coding in spiking neural networks. *arXiv preprint arXiv:2211.15386*, 2022.

- Lao-Rodríguez, A. B., Przewrocki, K., Pérez-González, D., Alishbayli, A., Yilmaz, E., Malmierca, M. S., and Englitz, B. Neuronal responses to omitted tones in the auditory brain: A neuronal correlate for predictive coding. *Science Advances*, 9(24):eabq8657, 2023.
- Lao-Rodríguez, A. B., Schröger, E., and Malmierca, M. S. The sound of silence: Omission responses and how the brain predicts in the absence of sound. *Neuroscience & Biobehavioral Reviews*, pp. 106505, 2025.
- Lee, K., Dora, S., Mejias, J. F., Bohte, S. M., and Pen-nartz, C. M. Predictive coding with spiking neurons and feedforward gist signaling. *Frontiers in Computational Neuroscience*, 18:1338280, 2024.
- Li, G., Deng, L., Tang, H., Pan, G., Tian, Y., Roy, K., and Maass, W. Brain-inspired computing: A systematic survey and future trends. *Proceedings of the IEEE*, 112(6):544–584, 2024. doi: 10.1109/JPROC.2024.3429360.
- Li, Y., Deng, S., Dong, X., Gong, R., and Gu, S. A free lunch from ann: Towards efficient, accurate spiking neural networks calibration. In *International Conference on Machine Learning*, pp. 6316–6325. PMLR, 2021.
- Liang, M. and Hu, X. Recurrent convolutional neural network for object recognition. In *Proceedings of the IEEE conference on computer vision and pattern recognition*, pp. 3367–3375, 2015.
- Liang, M., Hu, X., and Zhang, B. Convolutional neural networks with intra-layer recurrent connections for scene labeling. *Advances in neural information processing systems*, 28, 2015.
- Liao, Q. and Poggio, T. Bridging the gaps between residual learning, recurrent neural networks and visual cortex. *arXiv preprint arXiv:1604.03640*, 2016.
- Ma, D., Shen, J., Gu, Z., Zhang, M., Zhu, X., Xu, X., Xu, Q., Shen, Y., and Pan, G. Darwin: A neuromorphic hardware co-processor based on spiking neural networks. *Journal of systems architecture*, 77:43–51, 2017.
- Maass, W. Networks of spiking neurons: The third generation of neural network models. *Neural networks*, 10(9): 1659–1671, 1997.
- Masquelier, T. and Thorpe, S. J. Unsupervised learning of visual features through spike timing dependent plasticity. *PLoS computational biology*, 3(2):e31, 2007.
- Masquelier, T., Guyonneau, R., and Thorpe, S. J. Spike timing dependent plasticity finds the start of repeating patterns in continuous spike trains. *PloS one*, 3(1):e1377, 2008.
- Masquelier, T., Guyonneau, R., and Thorpe, S. J. Competitive stdp-based spike pattern learning. *Neural computation*, 21(5):1259–1276, 2009.
- Neftci, E. O., Mostafa, H., and Zenke, F. Surrogate gradient learning in spiking neural networks: Bringing the power of gradient-based optimization to spiking neural networks. *IEEE Signal Processing Magazine*, 36(6):51–63, 2019.
- Pei, J., Deng, L., Song, S., Zhao, M., Zhang, Y., Wu, S., Wang, G., Zou, Z., Wu, Z., He, W., et al. Towards artificial general intelligence with hybrid tianjic chip architecture. *Nature*, 572(7767):106–111, 2019.
- Rueckauer, B., Lungu, I.-A., Hu, Y., Pfeiffer, M., and Liu, S.-C. Conversion of continuous-valued deep networks to efficient event-driven networks for image classification. *Frontiers in Neuroscience*, 11, 2017. ISSN 1662-453X. doi: 10.3389/fnins.2017.00682.
- Sacramento, J., Ponte Costa, R., Bengio, Y., and Senn, W. Dendritic cortical microcircuits approximate the back-propagation algorithm. *Advances in neural information processing systems*, 31, 2018.
- SanMiguel, I., Widmann, A., Bendixen, A., Trujillo-Barreto, N., and Schröger, E. Hearing silences: human auditory processing relies on preactivation of sound-specific brain activity patterns. *Journal of Neuroscience*, 33(20):8633–8639, 2013.
- Shrestha, S. B. and Orchard, G. Slayer: Spike layer error reassignment in time. *Advances in neural information processing systems*, 31, 2018.
- Spratling, M. W. A review of predictive coding algorithms. *Brain and cognition*, 112:92–97, 2017.
- Tang, G., Kumar, N., Yoo, R., and Michmizos, K. Deep reinforcement learning with population-coded spiking neural network for continuous control. In *Conference on Robot Learning*, pp. 2016–2029. PMLR, 2021.
- Todorov, E. Convex and analytically-invertible dynamics with contacts and constraints: Theory and implementation in mujoco. In *2014 IEEE International Conference on Robotics and Automation*, pp. 6054–6061. IEEE, 2014.
- Todorov, E., Erez, T., and Tassa, Y. Mujoco: A physics engine for model-based control. In *2012 IEEE/RSJ International Conference on Intelligent Robots and Systems*, pp. 5026–5033. IEEE, 2012.
- Urbanczik, R. and Senn, W. Learning by the dendritic prediction of somatic spiking. *Neuron*, 81(3):521–528, 2014.

- Wang, S., Cheng, T. H., and Lim, M.-H. Ltmd: learning improvement of spiking neural networks with learnable thresholding neurons and moderate dropout. *Advances in Neural Information Processing Systems*, 35:28350–28362, 2022.
- Wu, Y., Deng, L., Li, G., Zhu, J., and Shi, L. Spatio-temporal backpropagation for training high-performance spiking neural networks. *Frontiers in neuroscience*, 12: 331, 2018.
- Xu, Z., Bu, T., Hao, Z., Ding, J., and Yu, Z. Proxy target: Bridging the gap between discrete spiking neural networks and continuous control. *arXiv preprint arXiv:2505.24161*, 2025a.
- Xu, Z., Shi, X., Dong, Y., Huang, Z., and Yu, Z. Care-bn: Precise moving statistics for stabilizing spiking neural networks in reinforcement learning. *arXiv preprint arXiv:2509.23791*, 2025b.
- Yao, M., Hu, J., Zhou, Z., Yuan, L., Tian, Y., Xu, B., and Li, G. Spike-driven transformer. *Advances in neural information processing systems*, 36:64043–64058, 2023.
- Yao, X., Li, F., Mo, Z., and Cheng, J. Glif: A unified gated leaky integrate-and-fire neuron for spiking neural networks. *Advances in Neural Information Processing Systems*, 35:32160–32171, 2022.
- Yaron, A., Shiramatsu-Isoguchi, T., Kern, F. B., Ohki, K., Takahashi, H., and Chao, Z. C. Auditory cortex neurons that encode negative prediction errors respond to omissions of sounds in a predictable sequence. *PLoS biology*, 23(6):e3003242, 2025.
- Yin, B., Corradi, F., and Bohté, S. M. Effective and efficient computation with multiple-timescale spiking recurrent neural networks. In *International Conference on Neuro-morphic Systems 2020*, pp. 1–8, 2020.
- Yin, L., Zheng, R., Ke, W., He, Q., Zhang, Y., Li, J., Wang, B., Mi, Z., Long, Y.-s., Rasch, M. J., et al. Autapses enhance bursting and coincidence detection in neocortical pyramidal cells. *Nature communications*, 9(1):4890, 2018.
- Zenke, F. and Ganguli, S. Superspike: Supervised learning in multilayer spiking neural networks. *Neural computation*, 30(6):1514–1541, 2018.
- Zhou, C., Zhang, H., Zhou, Z., Yu, L., Huang, L., Fan, X., Yuan, L., Ma, Z., Zhou, H., and Tian, Y. Qkformer: Hierarchical spiking transformer using qk attention. *Advances in Neural Information Processing Systems*, 37: 13074–13098, 2024.
- Zhou, Z., Zhu, Y., He, C., Wang, Y., Yan, S., Tian, Y., and Yuan, L. Spikformer: When spiking neural network meets transformer. *arXiv preprint arXiv:2209.15425*, 2022.

## A. Results on CIFAR10 Dataset

### A.1. Results on CIFAR10Net

This Cifar10Net spiking neural network architecture consists of the following components in sequence: an initial convolutional block (Conv2d(3, 128, kernel size=3, padding=1) + BatchNorm2d(128) + spiking neuron), followed by MaxPool2d(2,2); then two convolutional blocks—first Conv2d(128, 256, 3×3) and then Conv2d(256, 256, 3×3), each equipped with batch normalization and a spiking neuron, followed by another MaxPool2d(2,2); next, three identical deeper convolutional blocks (Conv2d(256, 512, 3×3) + BN + neuron); after flattening the feature maps, the data passes through two fully connected layers, the first being Linear(512×8×8, 512) with a neuron, and the second Linear(512, 10) with a neuron, to produce 10-class spiking outputs; finally, a global average pooling operation nn.AvgPool1d(10, 10) is applied along the temporal dimension to generate the final prediction. Training and testing curve in shown in Figure 6.

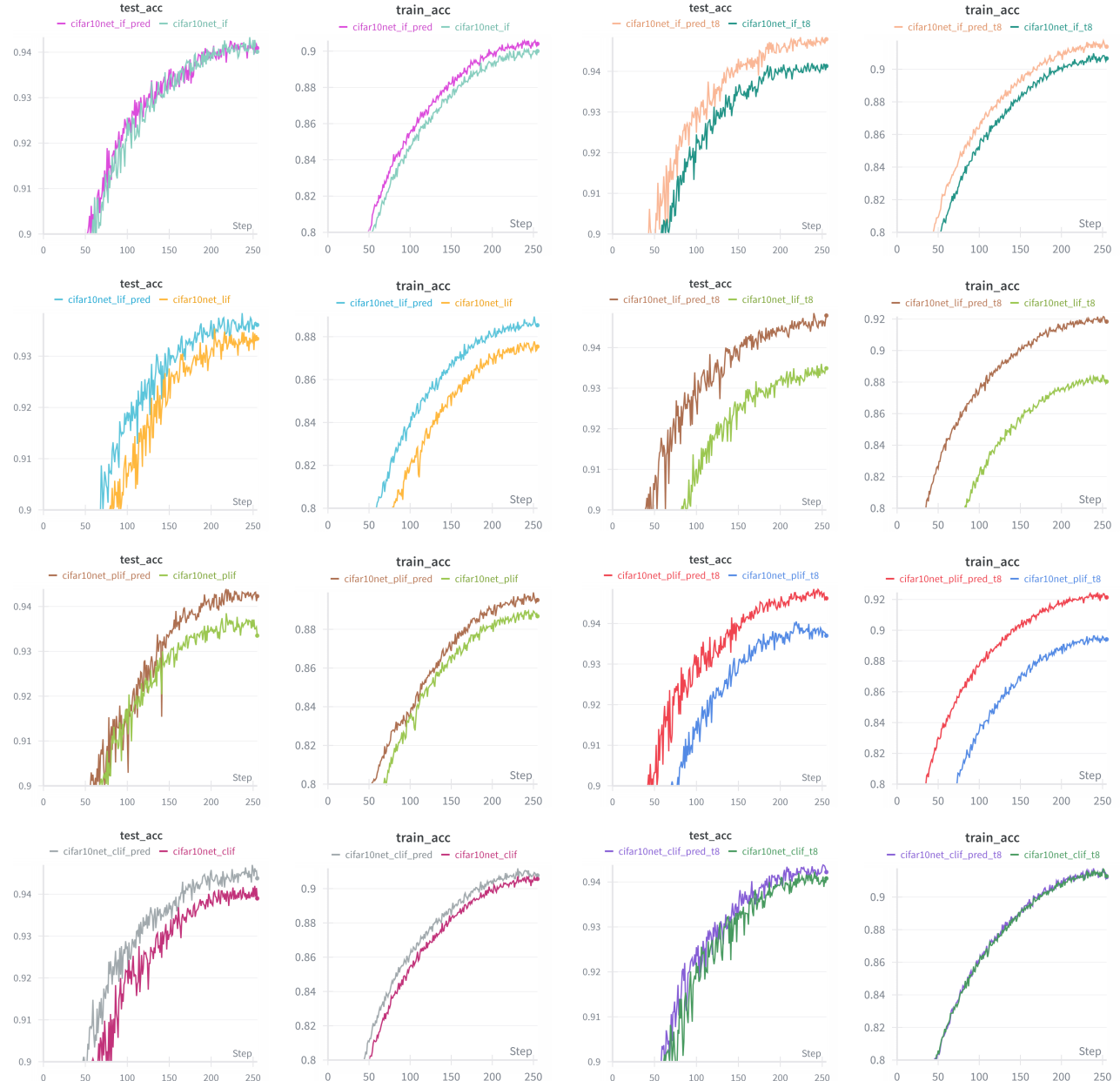


Figure 6. The training and testing accuracy curves of the CIFAR10Net trained with IF,LIF,PLIF and CLIF neurons along with their variants enhanced by self-prediction mechanisms at time-steps T=4 and T=8.

## A.2. Results on SEW ResNet

For the SEW ResNet families which is originally designed for ImageNet, when adapting them to CIFAR-10, we modify the first convolutional layer parameters, changing kernel size, stride, and padding from 7, 2, 3 to 3, 1, 1, respectively, and replace the initial max pooling layer with an identity mapping. Figure 7 shows the training and testing accuracy curve on SEW ResNet18. Figure 8 shows the training and testing accuracy curve on SEW ResNet34.

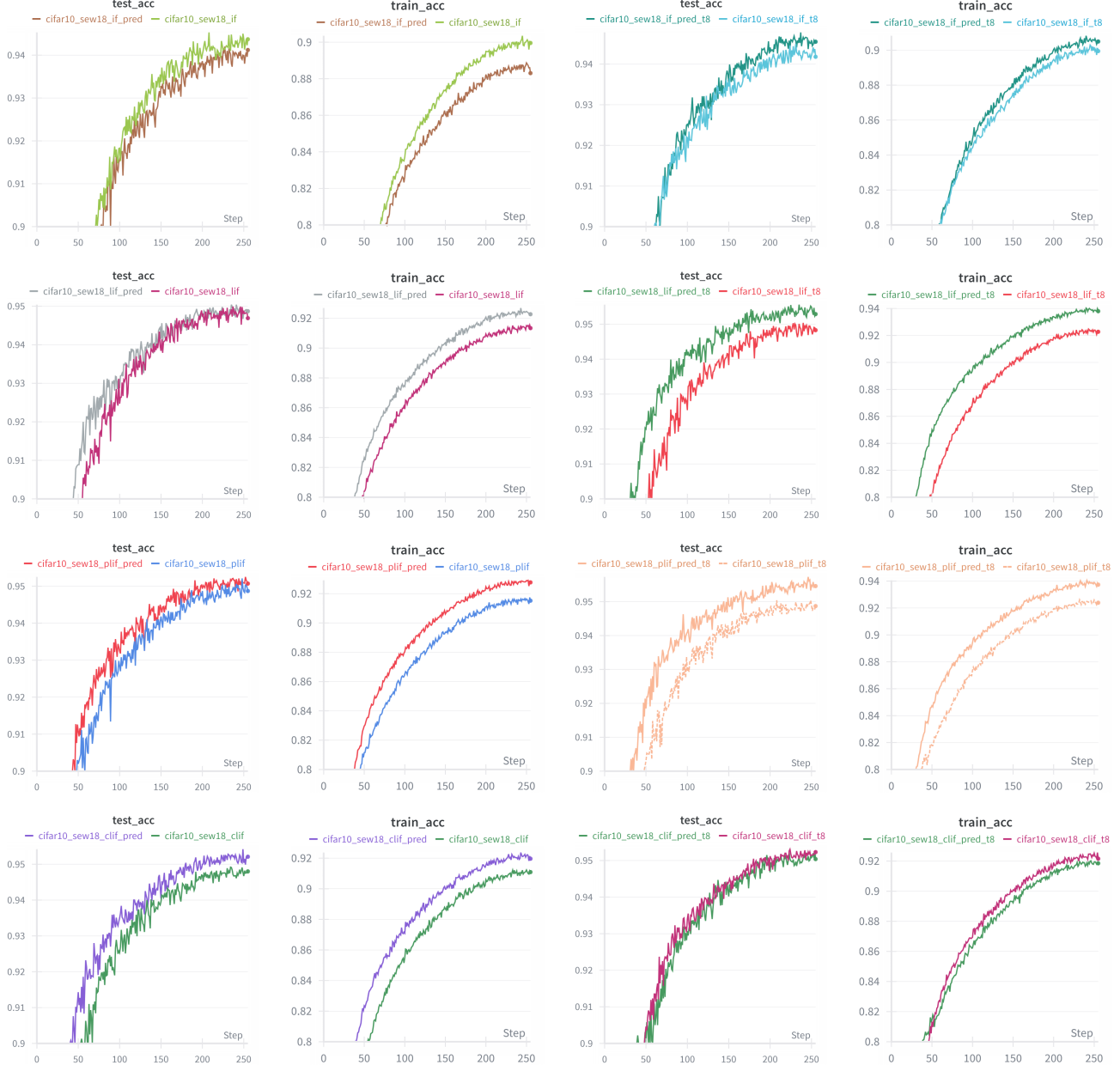


Figure 7. The training and testing accuracy curves of the SEW ResNet18 trained on CIFAR10 dataset with IF,LIF,PLIF and CLIF neurons along with their variants enhanced by self-prediction mechanisms at time-steps T=4 and T=8.

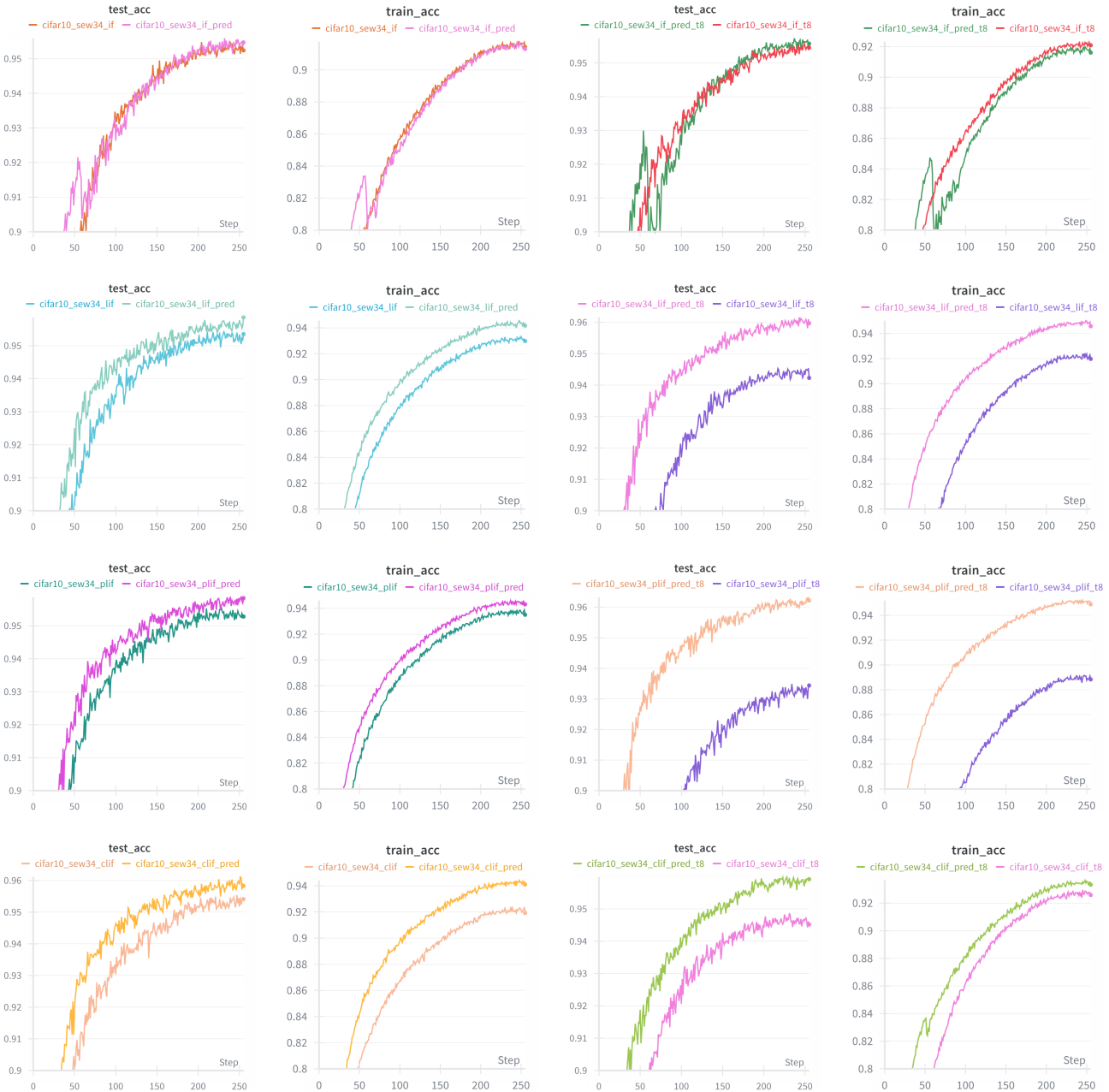


Figure 8. The training and testing accuracy curves of the SEW ResNet34 trained on CIFAR10 dataset with IF,LIF,PLIF and CLIF neurons along with their variants enhanced by self-prediction mechanisms at time-steps T=4 and T=8.

### A.3. Results on Spiking ResNet

For the Spiking ResNet families which is originally designed for ImageNet, when adapting them to CIFAR-10, we also modify the first convolutional layer parameters, changing kernel size, stride, and padding from 7, 2, 3 to 3, 1, 1, respectively, and replace the initial max pooling layer with an identity mapping. Figure 9 shows the training and testing accuracy curve on Spiking ResNet18. Figure 10 shows the training and testing accuracy curve on Spiking ResNet34.

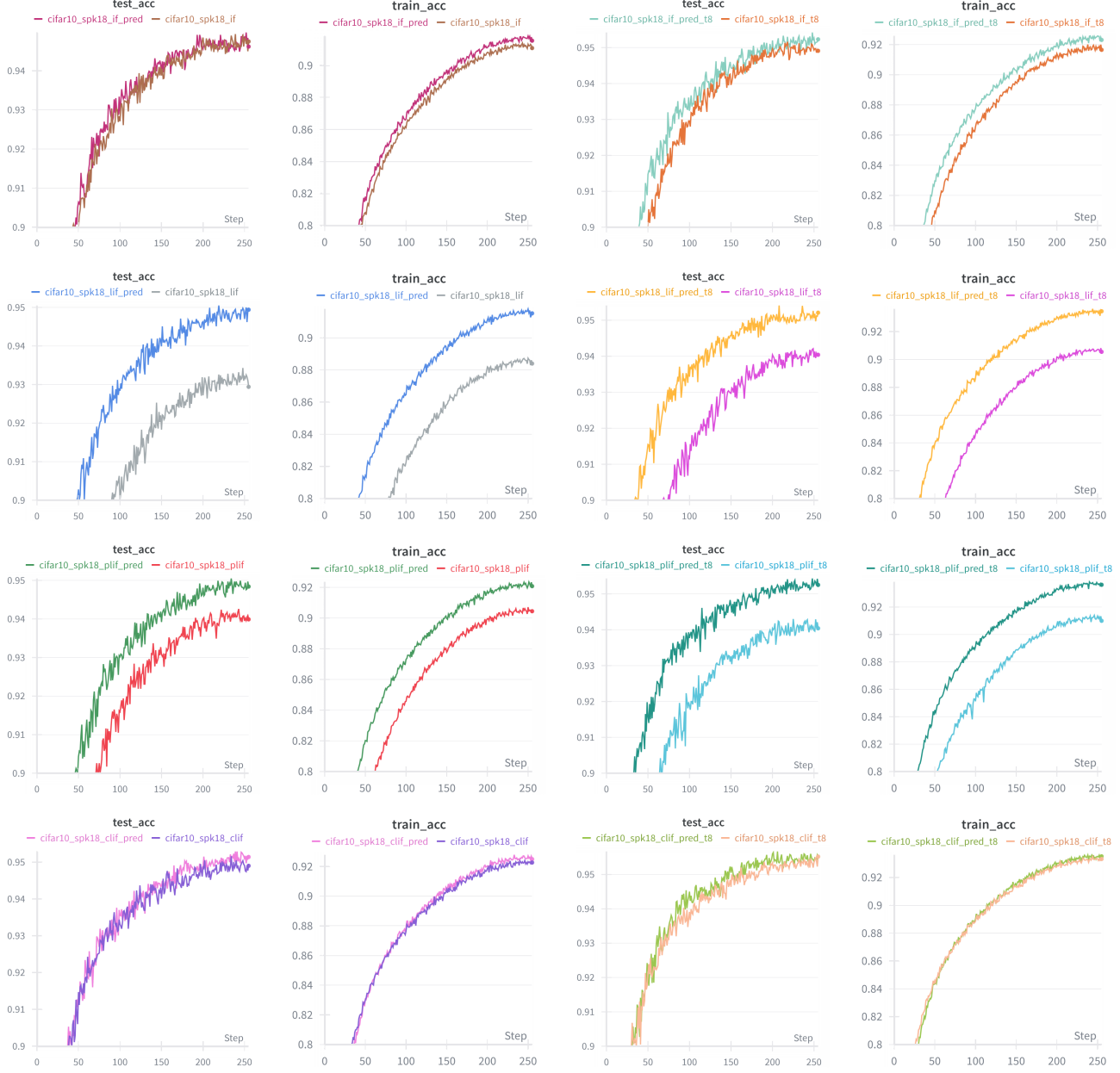


Figure 9. The training and testing accuracy curves of the Spiking ResNet18 trained on CIFAR10 dataset with IF,LIF,PLIF and CLIF neurons along with their variants enhanced by self-prediction mechanisms at time-steps T=4 and T=8.

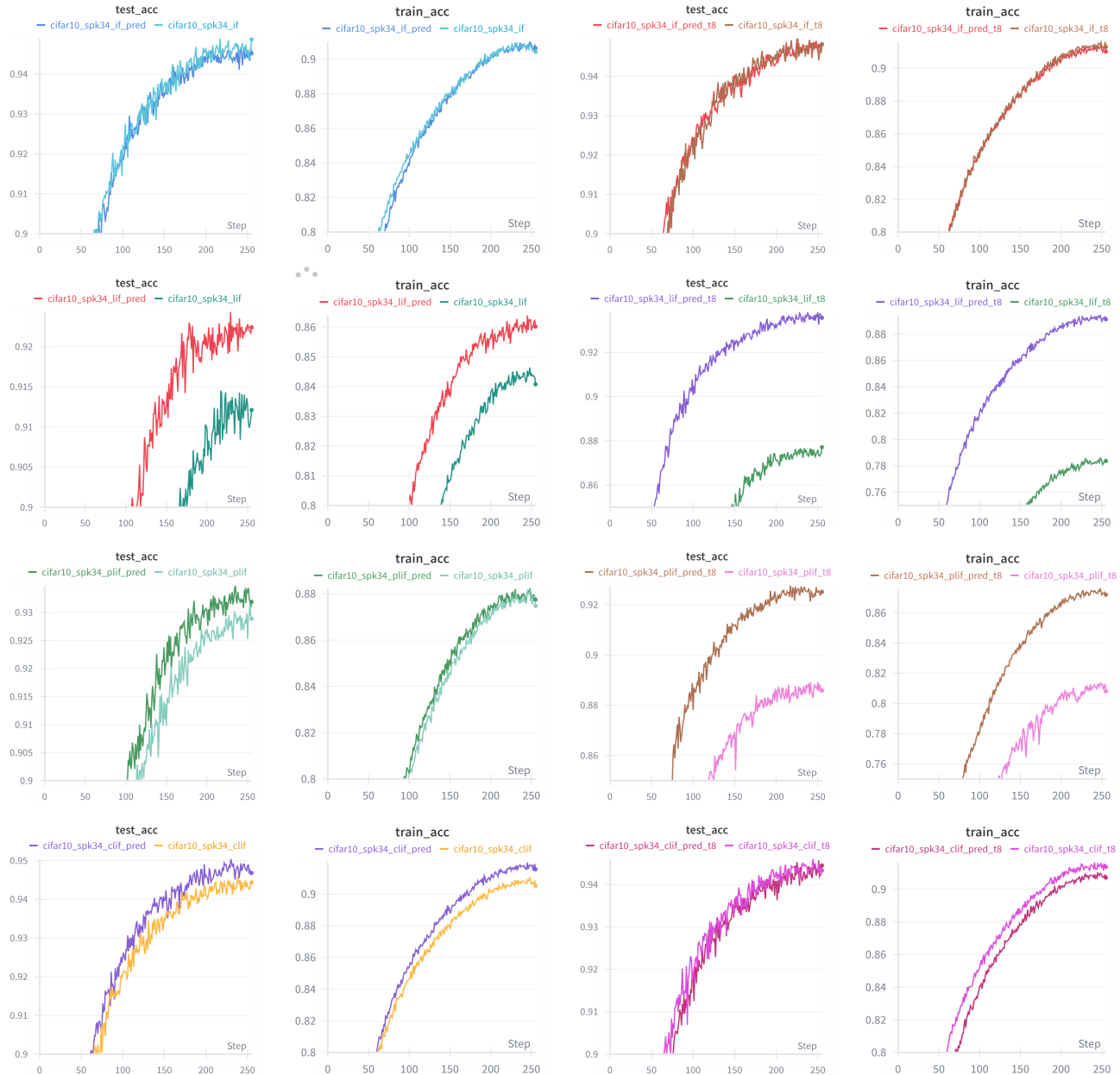


Figure 10. The training and testing accuracy curves of the Spiking ResNet34 trained on CIFAR10 dataset with IF,LIF,PLIF and CLIF neurons along with their variants enhanced by self-prediction mechanisms at time-steps T=4 and T=8.

## B. Results on ImageNet100 and ImageNet1k Dataset

Due to computational resource constraints, we evaluated the performance gains of the self-prediction enhancement method using the SEW ResNet-34 model on ImageNet-100 with both LIF and PLIF neurons. Additionally, we tested its effectiveness with PLIF neurons on the full ImageNet dataset using the SEW ResNet-18 model. The corresponding training and testing curves are shown in the Figure 11.

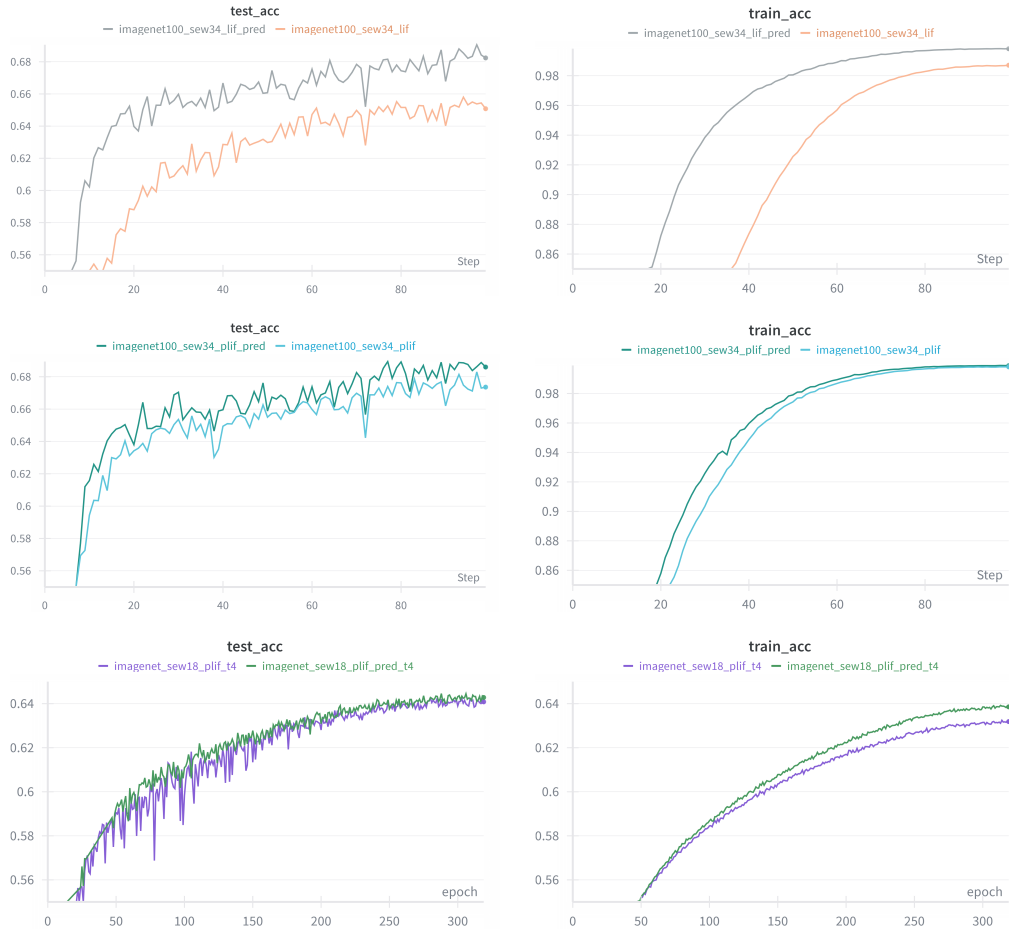


Figure 11. Training and testing accuracy curves on ImageNet100 and ImageNet dataset.

## C. Results on Sequential CIFAR10 Classification Tasks

For Sequential CIFAR10 Classification Tasks, we use our CIFAR10NetSeq architecture, which processes input images in a sequential manner by treating the spatial width dimension as time steps. It consists of the following components in sequence: two macro stages, each containing three convolutional blocks followed by an average pooling layer. Each convolutional block comprises Conv1d(inchannels, channels=128, kernelSize=3, padding=1, bias=False) to BatchNorm1d(128) to spiking neuron. The first block uses 3 input channels (RGB), while all subsequent blocks use 128 channels. After every three convolutional blocks, an AvgPool1d(2) reduces the temporal length by half. Following the convolutional stack, the feature sequence is flattened and passed through two fully connected layers: Linear(128  $\times$  8, 256) with a spiking neuron, then Linear(256, 10) without a neuron. Figure 12 shows the training and testing accuracy curve.

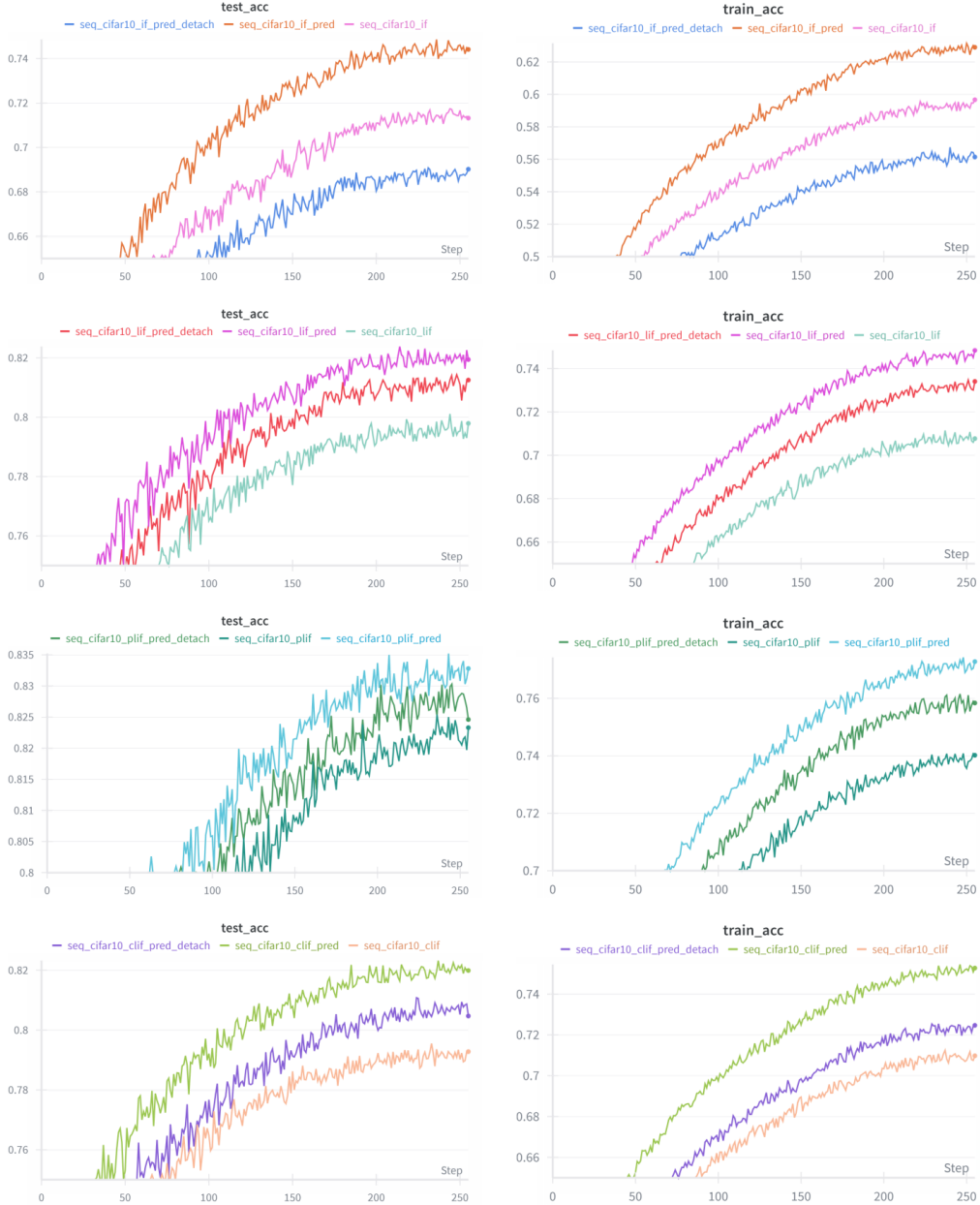


Figure 12. Training and testing accuracy curves on sequential CIFAR-10 using IF, LIF, PLIF, and CLIF neurons, including their self-prediction enhanced variants and an ablation on spike detachment in the computation of  $\mathbf{m}_p^l[t]$ .

## D. Experiment details of Reinforcement Learning Tasks

### D.1. Specific Parameters for the Proxy Target Framework

Table 5 lists the hyperparameters of the proxy target framework for different spiking neuron types. To better capture the dynamics of the SNN, the proxy network uses wider hidden layers than the corresponding online SNN. Because different spiking neurons exhibit distinct temporal dynamics and learning characteristics, both the hidden sizes and learning rates of the proxy network are adjusted accordingly across neuron types. All other hyperparameters remain identical.

*Table 5.* Hyper-parameters of the proxy network framework with different spiking neurons

Parameter	LIF
Proxy network architecture	(512, 512)
Proxy network activation	ReLU
Proxy network learning rate	$3 \cdot 10^{-3}$
Proxy network optimizer	Adam
Proxy update iterations $K$	1
Proxy update batch size $N$	256

### D.2. Spiking Actor Network Parameters

All hyperparameters of the spiking actor network are summarized in Table 6, following the same configuration as in a wide range of prior studies (Tang et al., 2021).

*Table 6.* Hyper-parameters of the spiking actor network

Parameter	Value
Encoder population per dimension $N_{in}$	10
Encoder threshold $V_E$	0.999
Network hidden units	(256, 256)
Decoder population per dimension $N_{out}$	10
Surrogate gradient window size $\omega$	0.5

### D.3. RL algorithm parameters

We conduct our experiments based on the TD3 algorithm (Fujimoto et al., 2018), using the hyperparameters listed in Table 7.

### D.4. Experiment environments

All environments were used with their default configurations without any modifications. Notably, since the state vector can take values in  $-\infty$  to  $\infty$ , it is normalized to the range  $(-1, 1)$  using a tanh function. Similarly, because actions are bounded by predefined minimum and maximum limits, the actor network's output is first passed through a tanh function to constrain it to  $(-1, 1)$ , and then linearly scaled to the actual action range (Min action, Max action).

Table 7. Hyper-parameters of the implemented TD3 algorithm (Fujimoto et al., 2018)

Parameter	Value
Actor learning rate	$3 \cdot 10^{-4}$
Actor regularization	None
Critic learning rate	$3 \cdot 10^{-4}$
Critic regularization	None
Critic architecture	(256, 256)
Critic activation	ReLU
Optimizer	Adam
Target update rate $\tau$	$5 \cdot 10^{-3}$
Batch size $N$	256
Discount factor $\gamma$	0.99
Iterations per time step	1.0
Reward scaling	1.0
Gradient clipping	None
Replay buffer size	$10^6$
Exploration noise $\mathcal{N}(0, \sigma)$	$\mathcal{N}(0, 0.1)$
Actor update interval $d$	2
Target policy noise $\mathcal{N}(0, \tilde{\sigma})$	$\mathcal{N}(0, 0.2)$
Target policy noise clip $c$	0.5